Proceedings of GT2005
ASME Turbo Expo 2005: Power for Land, Sea, and Air
June 6-9, 2005, Reno-Tahoe, Nevada, USA

GT2005-68264

Visualization of Rotor Endwall, Tip Gap, and Outer Casing Surface Flows In a Rotating Axial Turbine Rig

Nikhil M. Rao[1], Cengiz Camci[2]

Turbomachinery Heat Transfer Laboratory
Department of Aerospace Engineering
The Pennsylvania State University

223 Hammond Building, University Park, PA 16802

ABSTRACT

Visualization of surface flows in a large-scale, low speed, axial turbine rig was conducted using a visualization mixture of oil and pigment. Rotor endwall flows were visualized by applying a film of visualization material on the endwall. Tip surface flows were visualized by applying paint dots and oil film to the blade pressure surface. The visualization material is carried up on the blade surface due to rotation and some of the material seeps into the tip gap. The paint dot technique was used on blades with gap heights of 1.40% blade height and 0.72% blade height. Oil film visualization was used on blades with gap heights, as percent blade height, of 0.72%, 0.81%, 1.2%, and 1.40%. Outer casing boundary layer characteristics were also visualized by the oil film technique. Surface streamlines on the rotor endwall identify features such as saddle point, horseshoe vortex system, and skewed passage boundary layer. Tip surface streamlines indicate the presence of chord-wise flow on the tip surface, along with a distinct reattachment region. Variation of surface streamlines characteristics is correlated to the gap height. Outer casing surface streamlines show the variation in wall shear stress vector orientation through the rotor.

INTRODUCTION

Flow visualization is a qualitative technique used frequently to complement quantitative measurements in fluid dynamics. Its application to turbine flow fields, particularly in cascade facilities, has revealed many intricate details of flows specific to turbine blade passages. The most commonly used methods appear to be the use of smoke to visualize secondary flow structures, and the use of oil/pigment mixtures for surface flow visualization.

Wang et al [1] visualized the development of endwall secondary flows in a linear cascade using smoke wires and laser light sheet for illumination. A surface streamline technique using ink dots and oil of wintergreen film was introduced by Langston and Boyle [2] and applied to flow around a cylinder. This technique was also used by Aunapu et al [3] to investigate turbine passage endwall flows. A grid of ink dots was created on a contact using a permanent marker. The contact paper was then taped to a surface of interest and sprayed with a layer of solvent, oil of wintergreen. Ink dissolves in the alcohol and moves under the action of shear stresses when exposed to flow. Permanent record of the traces is available since the alcohol evaporates.

Flow visualization has also been applied to the problem of tip leakage flows. Sjolander and Cao [4] investigated flow patterns on the tip surface of an idealized blade in a wind tunnel. The blade, formed by a 90 circular arc, was used to simulate pressure-driven flow across the gap. Visualization of endwall and blade surface flows in a large scale rotating rig was carried out by Joslyn and Dring [5]. Surface streamlines were generated when gaseous ammonia discharged from surface static pressure taps reacted with Ozalid paper bonded to the surfaces. Allen and Kofskey [6] employed smoke to visualize the development of tip leakage and secondary flows in a low-speed rotating rig.

More recently, numerical simulations, for example Ameri and Bunker [7], Ameri et al [8], Prasad and Wagner [9], have also been used for the visualization of leakage flows.

While only a few examples of application of flow visualization to turbine flows have been cited, it is representative of the fact that majority of such efforts reported in the public domain have been carried out in linear cascade facilities. Measurements in a rotating rig are thus valuable for extrapolating these results with those that approach engine conditions. Visualization of surface flows on the rotor endwall, tip surface and outer casing surface is reported in this paper. To the authors' knowledge, the results presented in this paper, along with those in Rao and Camci [10] are the first such results obtained in a rotating rig. Observations of surface flow

1 *Research Assistant, Pennsylvania State University, nmr2@psu.edu*
2 *Professor of Aerospace Engineering, Pennsylvania State University, cxc11@psu.edu*

patterns in a rotating rig are compared to available literature, which in most cases is from cascade experiments.

EXPERIMENTAL SETUP & OPERATION

Turbine Research Facility: The facility used for the current research, shown in Figure (1), is the Axial Flow Turbine Research Facility (AFTRF), at The Pennsylvania State University. A detailed description of the design of this rig is available in Lakshminarayana et al [11], and Camci [12]. The turbine is a large-scale, low speed, cold turbine stage with many characteristics of modern high-pressure turbine stages. The total pressure and total temperature ratios across the stage are small and air flow through the facility is generated by a two-stage axial fan, located downstream of the turbine. The rotor hub extends 1.7 blade tip axial chord length beyond the rotor exit plane, as marked "Rotating Hub'" in Figure (1). Some of the important design performance data is listed in Table (1), while Table (2) lists important blade design parameters, including reaction at blade hub and tip sections. Blade velocity triangles at rotor tip and hub are shown in Figure (2).

The turbine rotor flow is low subsonic and hence does not account for compressibility effects, or the effects of shocks and expansion waves. The Reynolds number, based on exit relative velocity and actual chord, varies between $6*10^5$ and $7*10^5$ from hub to tip. These values are lower than those encountered in actual engines, probably by as much as an order of magnitude. However, they are in the range where it is expected that Reynolds number effects on boundary layer characteristics are adequately simulated. Additionally, flow through the tip gap is a function of the non-dimensional pressure difference, or the loading coefficient, that occurs across the blade tip. As noted in Lakshminarayana et al [11] the AFTRF blade was designed to have loading coefficient similar to high-pressure blades in actual engines.

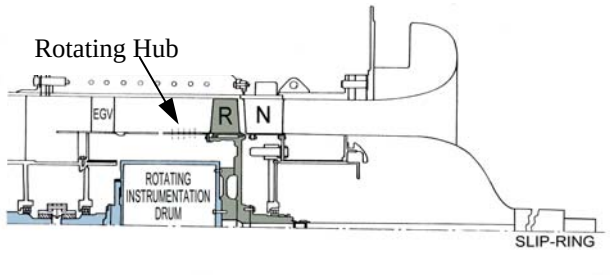

Figure 1 Axial Flow Turbine Research Facility (AFTRF)

Table 1 AFTRF Facility Design Performance Data

Inlet Total Temperature;T_{o1} (K)	289
Inlet Total Pressure;P_{o1} (kPa)	101.36
Mass Flow Rate;Q (kg/sec)	11.05
Rotational Speed; N (rpm)	1300
Total Pressure Ratio; P_{o1}/P_{o3}	1.0778
Total Temperature Ratio; T_{o3}/T_{o1}	0.981
Pressure Drop; P_{o1}-P_{o3} (mm Hg)	56.04
Power; P (kW)	60.6

Flow Visualization Technique: The visualization material used here consists of a mixture of oil and paint. The oil used was ash less dispersant, SAE 40 aviation oil (Aeroshell oil W 80). Two types of paint were used, a titanium white artists' oil color containing titanium oxide and zinc oxide pigments was used for oil film visualization. Paint dot visualization was done with a mixture of zinc oxide based yellow hue paint with the aviation oil. The visualization mixture contained equal parts by weight of oil and paint. This was necessitated by the fact that wall shear stress magnitudes encountered in the AFTRF are much higher than the measurements in low speed wind tunnels and linear cascades.

Table 2 AFTRF Stage Blade & Vane Data

Rotor hub-tip ratio	0.7269
Blade Tip Radius; R_{tip} (m)	0.4582
Blade Height; h (m)	0.1229
Exit Relative Mach Number (Tip)	0.24
Number of Blades	29
Tip Chord / Axial Tip Chord; (m)	0.1287 / 0.085
Turning Angle; Tip / Hub	95.42^o / 125.69^o
Nominal Tip Clearance; (mm)	0.9
Reaction, Hub / Tip	0.197 / 0.519
Reynolds # ($\div 10^5$) (based on true chord, exit relative velocities at hub and tip)	(6~7)

Operation: All surfaces were coated with a thin, smooth layer of flat black paint, prior to application of visualization material. Images of the treated surface were acquired to ensure reasonable repeatability in paint application between tests. The optical window was then fastened and the first fan stage was started. This brought the turbine to a stable speed of about 1240 rpm in approximately 30 seconds. The second fan stage was started at this time and in 30 seconds both the turbine rotor speed and flow rate were sufficiently stable. Thereafter, the rotor speed was increased to the corrected operating speed. Thus, the time required for the rotor to reach operating speed was less than 90 seconds in a total run time of about 20 minutes. A strobe light controlled by the AFTRF trigger pulse was used to conduct visual observations of the blades during the tests. This also assisted in determining run times and the test was terminated when no motion of visualization material was observed for 2 minutes.

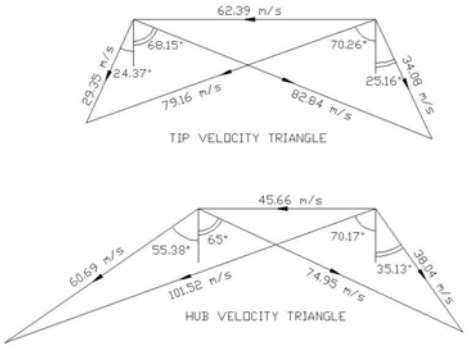

Figure 2 Blade Velocity Triangles at Tip and Hub

EXPERIMENTAL RESULTS & DISCUSSION

ROTOR PASSAGE ENDWALL FLOW VISUALIZATION

Oil film was applied uniformly on the endwall of two blade passages. Paint upstream of the leading edge was applied with a tangential orientation, while paint within the passage followed the general contour of the passage. The start-up procedure as explained previously was followed. Observations showed that the paint film was disturbed very little by the time the rotor reached operating conditions. It must also be noted that the patterns are formed over a long run time, about 20 minutes, and hence the effect of transients is believed to be washed out.

Visualization Around Blade Leading Edge

Figure (3) shows the surface flow features on the hub surface. The region of interest is upstream of the leading edge and around the leading edge. The patterns shown are due to flow in the rotating frame. Inlet flow stagnates as it approaches the blade leading edge, generating a saddle point region identified by the circle. The saddle point is identifiable since paint lines on the endwall show distinct regions of flow around this point, as indicated by the arrows. Flow immediately upstream of the saddle point is directed axially. Streamlines above and below the saddle point are directed away from the saddle point. The general orientation of streamlines implies that shear stresses in the boundary layer have a strong axial component, indicating that inlet boundary layer development is largely two-dimensional.

The location of the saddle point indicates that the flow close to the rotor hub approaches the blade at negative incidence. This behavior is consistent with the lower axial flow velocity within the boundary layer at nozzle exit, which would lead to negative incidence.

Flow around the leading edge displays the classical horseshoe vortex system, as proposed in secondary flow models such as Sharma and Butler [13], and Langston [14]. Streamlines due to the vortices have a distinctly different orientation than those caused by the inlet flow. On the suction side of the passage a continuous black line (H_S) is drawn to indicate the separation line between the suction-side leg of the horseshoe vortex and the inlet flow. Dotted curves drawn on either side of H_S indicates flow towards this line. Inlet flow is seen to turn into the passage and flow around the blade, while the stagnating flow is trapped in the vortex. Visualization material near the suction surface – endwall corner is seen to move in two directions.. Originating from about the same point, one streamline (dashed curve) indicates flow towards the blade surface while the other (dotted curve) indicates flow away from the blade surface. One explanation for this could be that after impinging near the blade corner the flow is initially towards the saddle point before the fluid turns towards the passage. More visualization material is also washed away from the passage endwall as inlet flow accelerates around the suction surface.

The pressure-side leg of the horseshoe vortex is also identified in Figure (3). This leg is more distinct because it moves out into the passage, rather than around the blade. Two continuous lines [H_P] are drawn to indicate the dividing streamlines between the pressure-side leg of the horseshoe vortex and surrounding flow. This suggests that the pressure-side leg of the horseshoe vortex is attached to the rotor endwall. There also appears to be a break in the dividing line closer to the pressure-side of the leading edge. Streamline patterns within the pressure-side leg vortex are similar to that observed for the suction-side leg. After impingement, on pressure-side of the passage, flow is first towards the saddle point before it turns towards the passage. The pressure-side leg appears to move in a straight line, except for a small shift away from blade pressure surface.

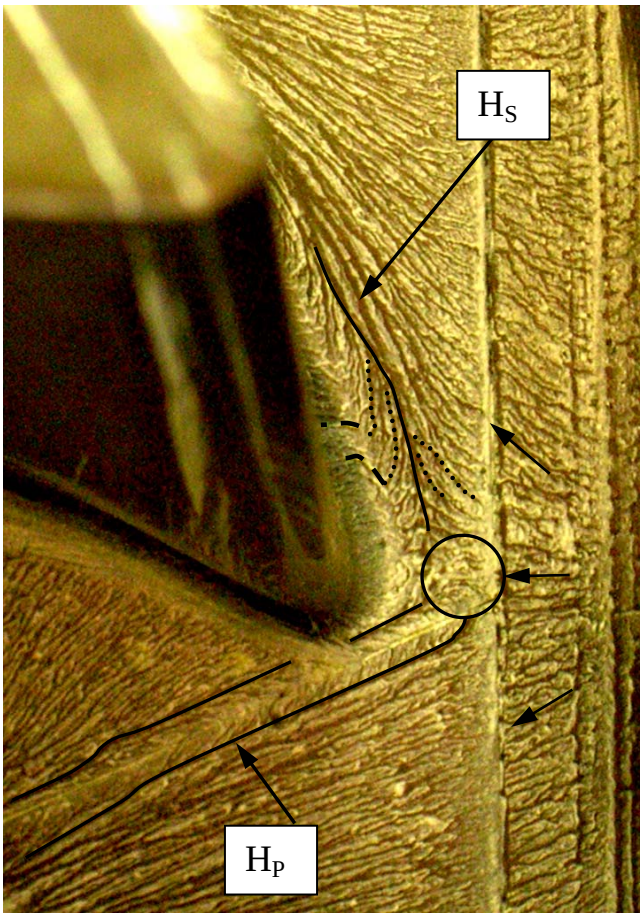

Figure 3 Details of Flow Patterns Around Blade Leading Edge

Visualization In Rotor Passage

An overall view of passage endwall surface flow is shown in Figure (4). The horseshoe vortex system is marked out in continuous lines. Near the point of maximum blade curvature there is considerable paint accumulation over a wide area, shown bounded by a dotted curve. This could result from reduced wall shear. From their respective trajectories it appears that the pressure-side leg impinges on the suction surface beyond the point of maximum curvature, while the suction-side leg separates from the endwall near the point of maximum curvature.. The cascade endwall flow structure discussed by Sharma and Butler [13] indicates that the suction-side leg of the horseshoe vortex separates from the endwall around the point of maximum blade curvature. Wang, et al [1] on the other hand show merging of the two legs of the horseshoe vortex near the point of maximum blade curvature.

Above the pressure-side leg of the horseshoe vortex the endwall boundary layer flow is entirely across the passage. This

highly skewed endwall boundary layer is also observed in cascade visualizations, for example, Gregory-Smith et al [15].

Near Trailing Edge Surface Flows

Figure (5) displays endwall surface flow patterns in the near trailing edge region of the blade passage. The secondary flow is seen to encompass the entire passage. The surface streamlines are oriented almost cross-passage. At rotor exit, flow from pressure surface to mid-pitch appears to exit the rotor at more or less the design relative flow angle of 65°, measurements from Figure (5) yield an angle of approximately 62°. From mid-pitch to the suction-side the streaks show some curvature as the flow turns towards the axis. The orientation indicates overturning experienced by the near endwall flow due to the effects of the passage vortex. The blade wake is identified in Figure (5) as a region of accumulation of visualization material. Visualization material tends to accumulate at the blade-endwall corners and might lead to the dense patch identified. Additionally, the wake fluid is low momentum, thus causing the accumulation to persist downstream of rotor exit plane.

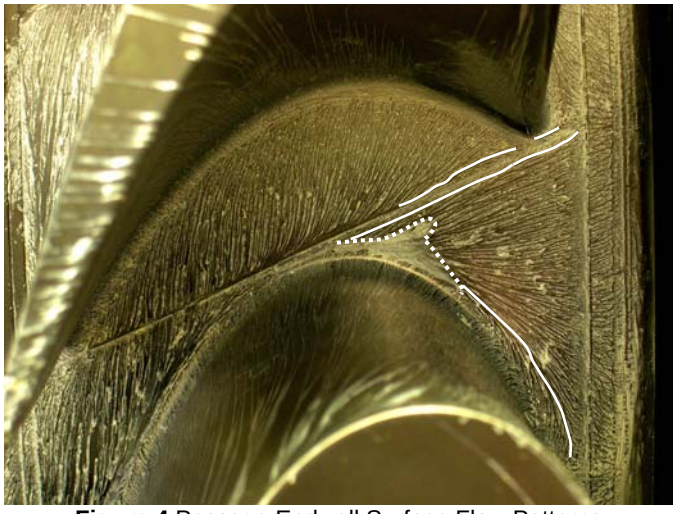

Figure 4 Passage Endwall Surface Flow Patterns

Images of Suction Surface

As a consequence of rotation, some visualization material is swept up the blade suction surface, as shown in Figure (6). No visualization material was applied to blade pressure surface. The paint lines on the suction surface are directed radially outwards with some curvature and smearing. This is consistent with the centrifugal force being the driving mechanism for the visualization material to move up the blade surface. The lines thus do not represent passage flow features, apart from being an indicator of the ratio of centrifugal force to aerodynamic shear imposed on the visualization material. The most significant observation is the large, comet-tail like, paint streak just below the blade tip, starting at about mid-chord and extending the length of the blade. This is very distinct from the other paint traces on the suction surface and displays remarkable continuity in paint deposition along the blade surface. The streak is believed to be caused by visualization material trapped in the tip leakage vortex. A very similar structure was shown to occur during visualization of tip surface flows in Rao and Camci [10].

The nature of deposition of visualization material indicates a highly unsteady flow structure. The trace of the leakage vortex begins after mid-chord (axial), close to the tip surface. The upper boundary of the trace displays a downward trajectory along the blade surface. The size of the streak increases with chordwise distance and it appears that the paint deposited decreases. Suction surface static pressure distributions conducted by Xiao, et al [16] in the AFTRF show a low pressure zone starting beyond mid-chord at about 95% span. This corresponds well with the observations made in the present study. Xiao, at al [16] also report a 21 angle between the trajectory of the tip vortex and the casing. At the trailing edge, the clear region above the streak measures about 10% blade height, while the width of the streak is about 13% blade height.

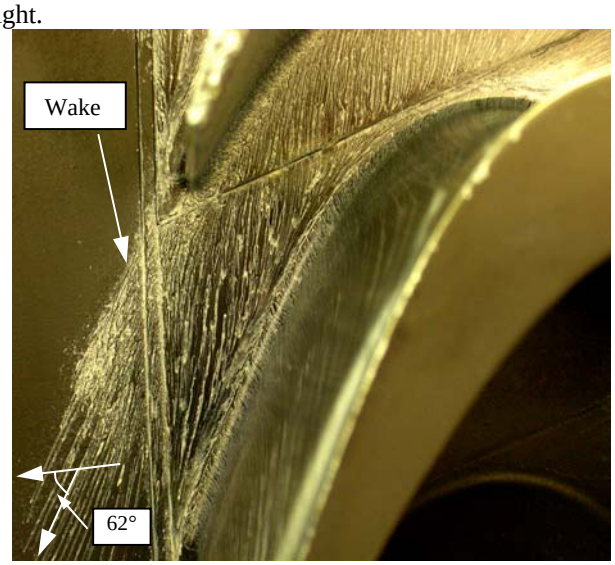

Figure 5 Near Trailing Edge Surface Flow Patterns

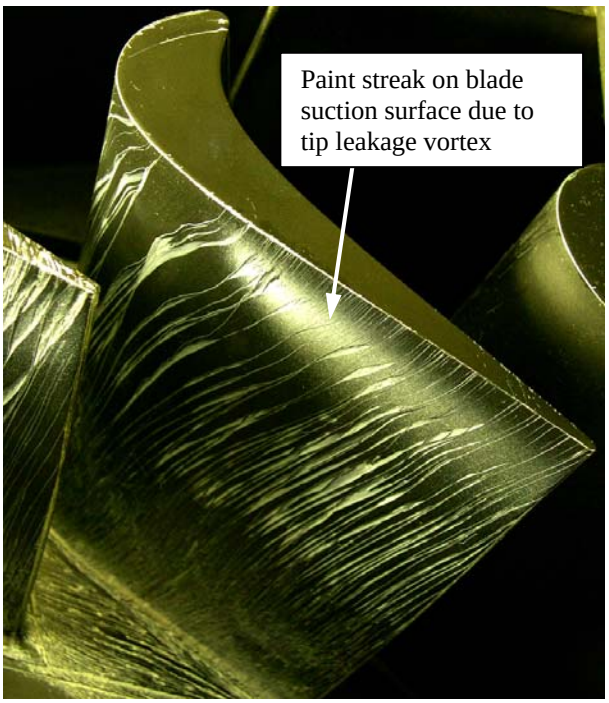

Figure 6 Suction Surface Patterns from Rotor Endwall Visualization

BLADE TIP SURFACE FLOW VISUALIZATION

Blade Tip Surface Flow Visualization by Paint Dots

Blade tip surface flow visualization was conducted by applying paint dots on the pressure surface of certain rotor blades. The visualization material moves up on the blade pressure surface under the action of centrifugal forces and is eventually thrown off the blade surface at the pressure-side corner. Some of this material is carried on to the tip surface by leakage flow entering the gap. Visualization material deposited on the tip surface forms surface streamlines under the action of wall shear stresses due to over tip leakage flow. Tests were conducted to ensure that the patterns were not formed on the tip surface before the rotor reached operating conditions. The results of these are not shown. The tests were conducted in three stages. In the first stage only one axial fan was turned on, for a total run time of two minutes. The second stage consisted of starting the second axial fan two minutes after the first was started and this test was run for a total of four minutes. In the final stage, procedure of stage two was repeated and at the end of four minutes the turbine rotor speed was increased to operating speed. The total run time in this case was six minutes. All tests were run back to back, with the same visualization mixture and all blade surfaces were cleaned prior to each test. The following observations were made; paint from the blade pressure-side reached the tip platform in the first stage, however very few streaks were formed. The number of surface lines increased for the second stage although the definition of the surface patterns was poor. The third stage showed the best definition in surface patterns and even greater amount of surface patterns that covered an area similar to the results shown in this paper. The results presented in this section are from run times of 20 minutes, as described in operation procedure.

Influence of Tip Gap Height

The tip surface patterns for blade with a gap height of t/h = 1.40% are shown in Figure (7). Also seen on the blade tip surface is a tip trench used for coolant injection as detailed in Rao and Camci [17, 18]. The trench is filled in with silicone sealant. All dot traces deposit material on to the tip surface, except close to the trailing edge. The paint lines on the pressure-side are distinct and directed radially outwards. The increased aerodynamic wall shear close to the trailing edge causes the paint to flow around the trailing edge and not reach the tip surface. A continuous, chordwise trace is formed on the tip surface, in spite of discrete paint deposition on the tip surface. This trace runs more or less parallel to the pressure-side edge of the tip gap and indicates a chordwise flow in the near pressure-side corner region of the tip surface. Flow visualization in an idealized tip gap by Sjolander and Cao [4] detected the presence of organized, chordwise flow in the separation region near the pressure-side corner. The trace is very close to the pressure-side corner over the first half of the blade and then moves towards the blade suction-side edge at about 55% C_{ax}. Coincidentally, paint streaks across the tip surface are seen to start at about the same chordwise location. At 60% C_{ax} the distance of the trace measured normal to the axial chord is about 3% C_{ax} from the pressure-side edge and about 1.4 times the gap height. Over the last 5% blade chord there is no trace. Tip surface visualization by Rao and Camci [10] showed that gap flow does not attach on the tip surface in this region, thereby eliminating the chordwise flow.

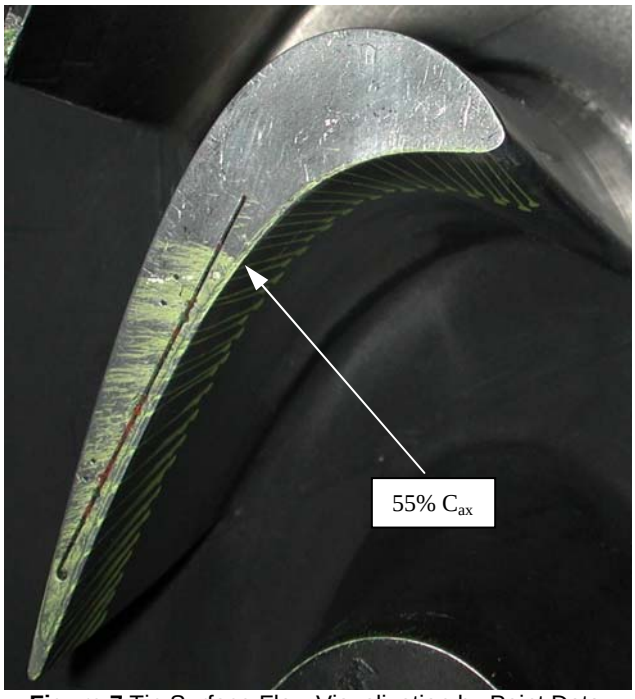

Figure 7 Tip Surface Flow Visualization by Paint Dots, Blade (t/h = 1.40%)

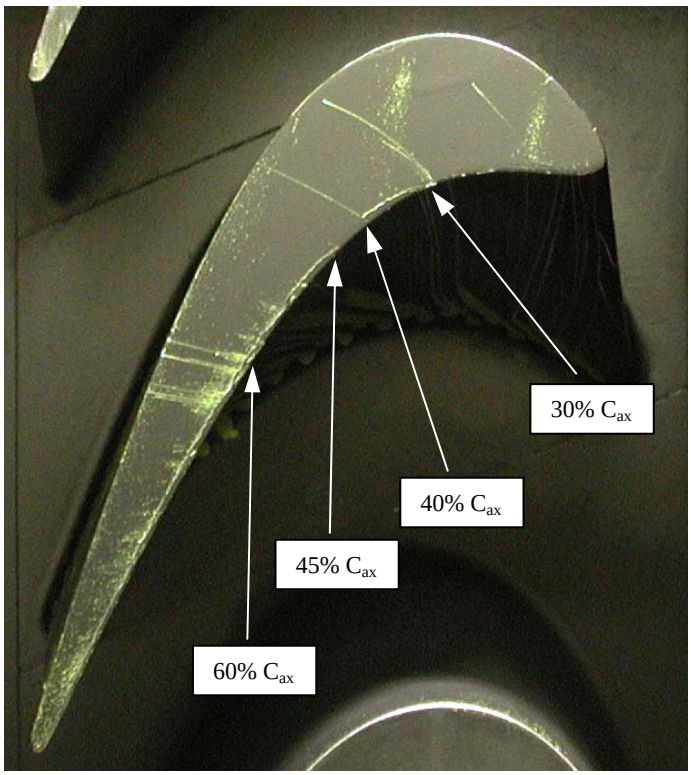

Figure 8 Tip Surface Flow Visualization by Paint Dots Near Blade Root, Blade (t/h = 0.72%)

Figure (8) shows tip surface patterns on the blade with t/h = 0.72%, At about 30% C_{ax} there is a curved streak that crosses

the tip surface, indicating that surface flow is being accelerated towards the suction-side edge of the tip gap. The chordwise flow line beginning from this point terminates at about 40% C_{ax} in a long straight streak. Beyond this point the chordwise line begins again at 45% C_{ax} and is continuous up to the trailing edge. The line is closer to the blade pressure-side corner, in comparison to the large gap height previously presented. At 60% C_{ax} the distance of the trace measured normal to the axial chord is about 1.1% C_{ax} from the pressure-side edge and about 1.1 times the gap height. The surface streamlines that start out from this line are intermittent, with a large amount of streamlines in the region 60% C_{ax} – 70% C_{ax}. Thus, the effect of decreasing the gap size is to confine the separated zone closer to the blade pressure-side edge.

Blade Tip Surface Flow Visualization by Oil Film

Tip surface flow visualization with oil film on the blade pressure side was conducted in order to identify detailed surface flow features on the tip surface. The procedure is explained in Rao and Camci [10]. Briefly, the film applied to the blade pressure-side is subject to centrifugal forces due to rotation and is forced up the blade surface. As in the paint dot technique the visualization material is carried on to the tip platform by the gap flow. The paint deposition tends to be greater and more continuous.

Blades with gap heights of 0.72%, 0.81%, 1.2%, and 1.40% were tested and the surface flow patterns are presented in Figure (9) through Figure (12) respectively. Some of the important flow features that are identified in the figures are pressure-side corner paint accumulation due to separated flow, reattachment of gap flow on the tip surface, and a recirculation region. Visualization on three different blades, with gap heights of 0.72%, 0.81%, and 1.40%, was conducted in a single test run. The gap height of 1.40% was varied using precision plastic layers and double-sided tape to obtain the gap height t/h = 1.2%. The figures show a sector of the tip surface between 50% C_{ax} and 75% C_{ax} and are scaled up equally. This allows for a direct comparison of the various gap heights.

Figure (9), shows considerable paint accumulation near the pressure-side corner on the tip surface of blade with gap height t/h = 0.72%. This accumulation is partly due to low momentum activity in the separated flow over the tip surface and partly deposition of visualization material by the recirculating flow. The definition of the recirculating flow streamlines improves as the gap height is increased, as observed in Figure (10) through Figure (12) for blades with gap heights of t/h = 0.81%, 1.2%, and 1.40% respectively. The extent of paint accumulation from the pressure-side edge of the tip surface does not change much with increase in gap height. It is also clear from the figures that at the smaller gap heights the recirculation patterns on the tip surface start closer to blade leading edge. The reattachment line however moves farther away from the pressure-side corner and Figure (13) shows the measured position of the reattachment line from the pressure-side corner as a function of gap height. The measurements normal to blade tip axial chord (solid square symbols) and normal to camber line (solid circle symbols) were taken from the images. In both cases the curve-fit implemented is quite linear. It must be noted that the difference between t/h = 0.72% and t/h = 0.81% was smaller than that could be measured. When the gap height is almost doubled from t/h = 0.72% to t/h = 1.40%, the reattachment line moves from 5% C_{ax} to 10% C_{ax} as measured normal to the axial chord. It is generally accepted in the literature that over tip leakage behavior varies linearly with gap size. Reattachment distance measured normal to axial chord and normalized by gap height (solid triangles) is fairly invariant with gap height. The value lies between 1.95t and 2t. The outlier is at gap height t/h = 0.81% and again this is believed to be due to resolution of measurement.

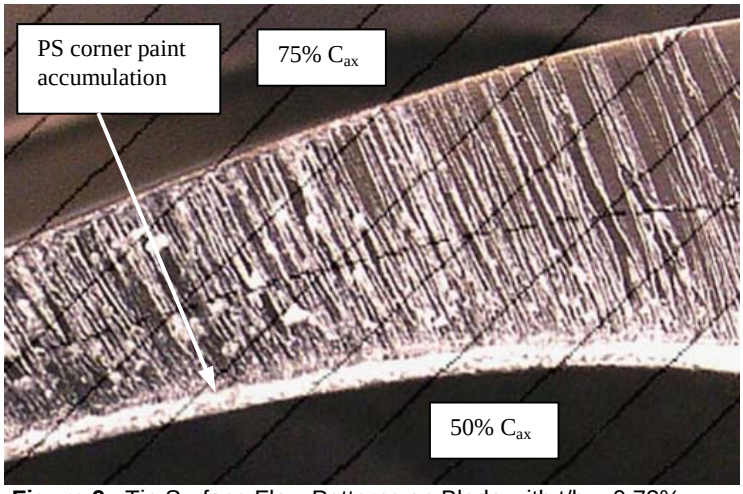

Figure 9 Tip Surface Flow Patterns on Blade with t/h = 0.72%

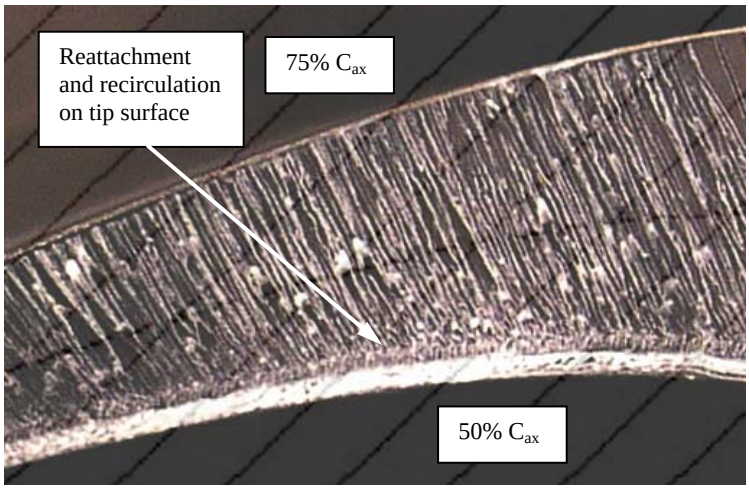

Figure 10 Tip Surface Flow Patterns on Blade with t/h = 0.81%

ROTOR CASING SURFACE FLOW VISUALIZATION

Rotor casing surface flow was visualized by using the oil film technique. This is believed to be the first such effort in a rotating rig. Figure (14) shows the oil film applied to the casing surface. The visualization material was applied using a soft brush with an axial orientation. Visible rotor blades and nozzle vane are marked in Figure (14).

An image of the outer casing flow patterns taken after the test was completed and rotor was stopped is shown in Figure (15). The surface streamlines indicate that up to about mid-chord the tangential and axial components of wall shear stresses are about equal and directed in the direction of rotation. A region of decreased shear is identified by a pair of white dotted lines. The fluid in this region appears to originate from

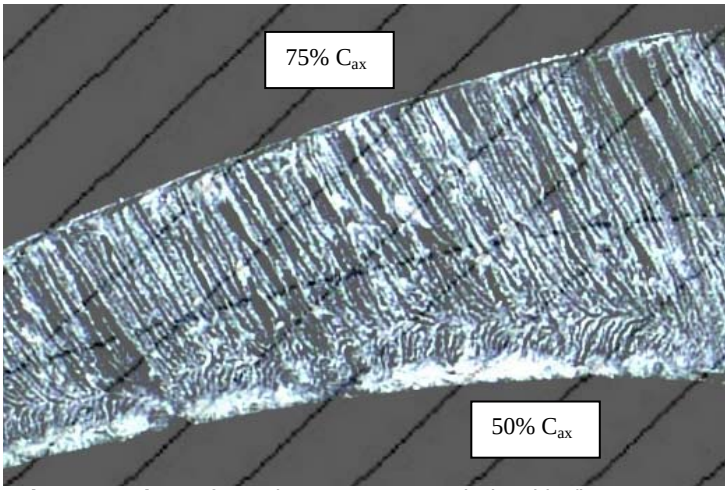

Figure 11 Tip Surface Flow Patterns on Blade with t/h = 1.2%

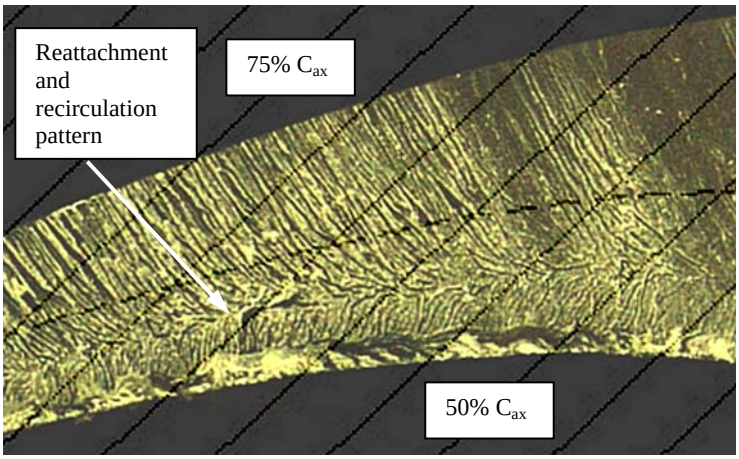

Figure 12 Tip Surface Flow Patterns on Blade with t/h = 1.40%

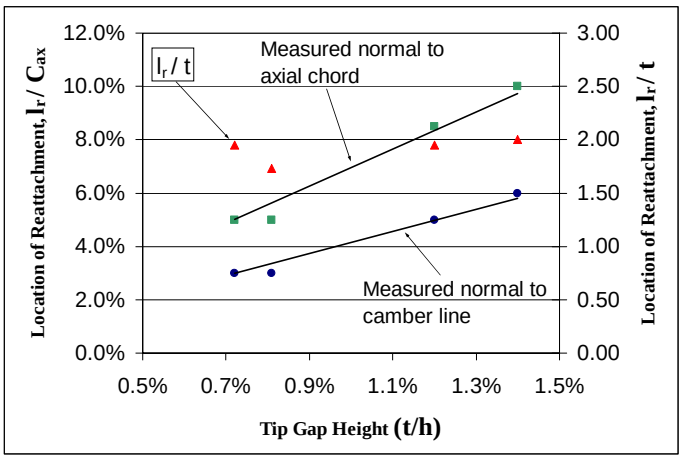

Figure 13 Location of Reattachment on Tip Surface as a Function of Tip Gap Height.

the suction side of the preceding nozzle guide vane. The low momentum region appears to persist until about mid-chord. There is negligible streamline curvature up to about mid-chord, beyond which the streamlines are continuously curved till the rotor exit. Downstream of rotor exit there are regions of differing paint accumulation. Surface streamlines leading into region **A** appear to cover the greatest distance, carrying more visualization material. It is clear from this picture that the wall shear imposed on the visualization material is significantly larger in the footprint of the rotor than downstream of the rotor.

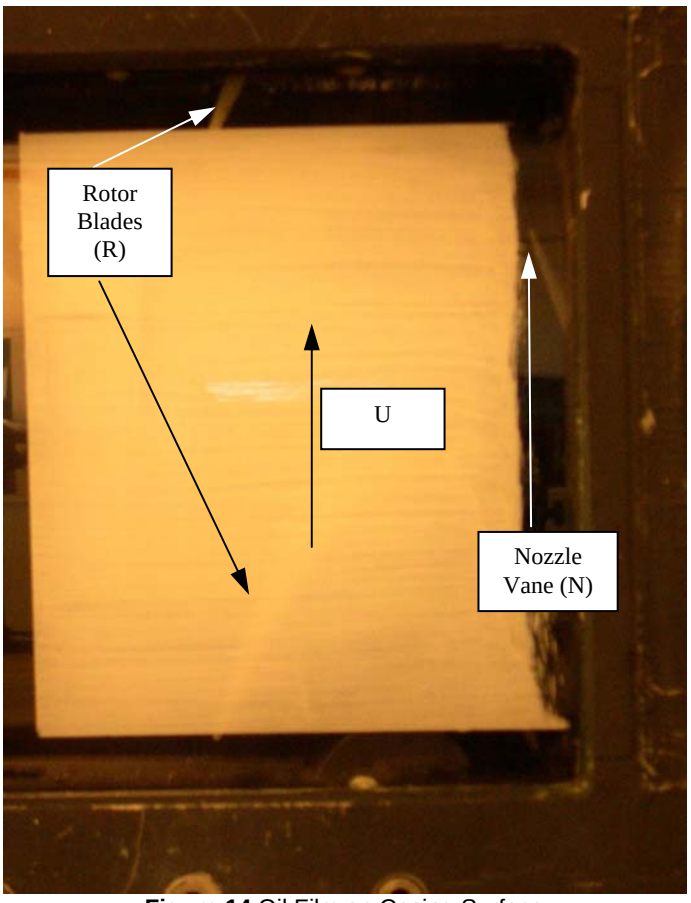

Figure 14 Oil Film on Casing Surface

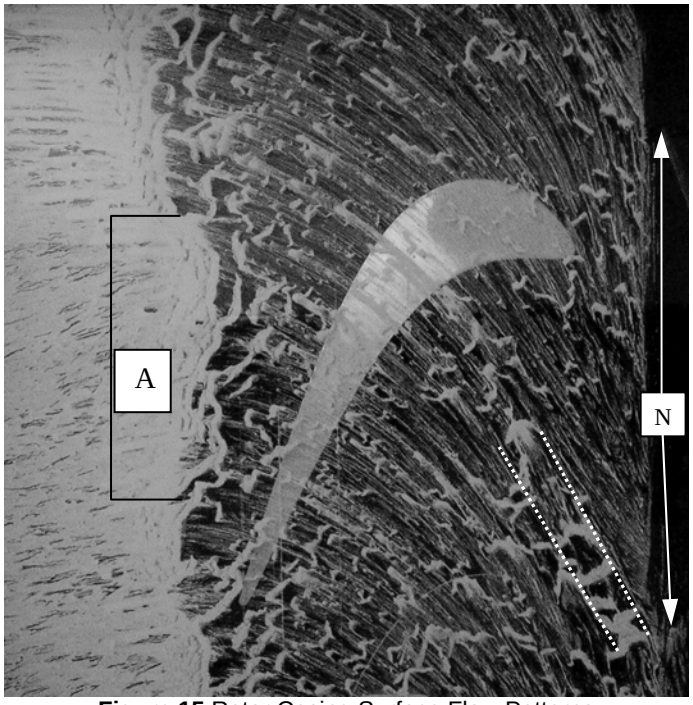

Figure 15 Rotor Casing Surface Flow Patterns

CONCLUSIONS

Visualization of rotor endwall, tip surface, and rotor casing flows was conducted in a large scale, rotating axial turbine rig, by using an oil and paint technique.

Rotor endwall surface flow visualization successfully identified features such as the saddle point upstream of the leading edge, the horseshoe vortex system, and strong cross-passage flows that result in the passage vortex.. Unique to this study is the identification of the trace of the tip leakage vortex seen on the blade suction surface. This was possible since the visualization material is carried radially outwards along the suction surface due to rotation.

Tip surface visualization was conducted on blades with different tip gap heights. A continuous chordwise trace of visualization material on the tip surface indicates the chordwise flow present in the separated flow region near the pressure-side edge. This trace moved closer to the pressure-side edge as gap height was decreased. A distinct reattachment line was also identified on the tip surface. The location of this line, measured from the pressure-side corner was found to increase linearly with gap height. The point of reattachment measured normal to axial chord and normalized by tip gap height appears to vary little with gap height.

Outer casing surface flows were visualized using a transparent casing. A region of low momentum, originating from the suction side of preceding nozzle vane appears to persist up to rotor tip mid-chord. The average shear stress direction on the casing at rotor inlet has a strong tangential component in the direction of rotation. This changes gradually through the rotor, to an almost axial orientation at rotor exit.

Flow visualization indicating local separation and reattachment may be very illuminating in explaining heat transfer results on the rotor surface.

The visualized flow patterns can be helpful is assessing present day viscous flow solvers, since numerical equivalents of surface oil flow patterns can be readily obtained during post processing of numerical data.

ACKNOWLEDGMENTS

The authors would like to thank Auhl, R., and Catalano, M., in the Department of Aerospace Engineering at Penn State and Houtz, H., for his assistance with facility maintenance.

NOMENCLATURE

C_{ax}	Rotor tip axial chord length, m
h	Rotor blade height, m
$p_{o1,}$ P_{o1}	Stage inlet total pressure, Pa
$p_{o3,}$ P_{o3}	Stage exit total pressure, Pa
t	Gap height between blade tip and outer casing, m
l_r	Distance of reattachment line from pressure-side corner, m

REFERENCES

1. Wang, H. P., Olson, S. J., Goldstein, R. J., and Eckert, E. R. G., 1995, "Flow Visualization in a Linear Turbine Cascade of High Performance Turbine Blades," *ASME* Paper No. 95-GT-7.
2. Langston, L. S., and Boyle, M. T., 1982, "A New Surface-Streamline Flow Visualization Technique," J. Fluid Mech., **125**, pp. 53-57.
3. Aunapu N V., Volino R J., Flack K A., and Stoddard R M., 2000, *ASME* J. Turbomachinery, **122**, pp. 651-658.
4. Sjolander, S. A., and Cao, D., 1995, "Measurements of flow in an idealized turbine tip gap," *ASME* J. Turbomachinery, **117**, pp. 578-584
5. Joslyn, H. D., and Dring, R. P., 1990, "Three-Dimensional Flow in an Axial Turbine. Part 1-Aerodynamic Mechanisms," *ASME* Paper No. 90-GT-56.
6. Allen, H. W., and Kosfskey, M. G., *Visualization Study of Secondary Flows in Turbine Rotor Tip Regions. NACA* TN-3519.
7. Ameri, A. A., and Bunker, R. S., 2000, "Heat Transfer and Flow on the First-Stage Blade Tip of a Power Generation Gas Turbine: Part 2-Simulation Results," *ASME* J. Turbomachinery, **122**, pp. 272-277, Paper No. 99-GT-283.
8. Ameri, A. A., Steinthorsson, E., and Rigby, D. L., 1999, "Effects of Tip Clearance and Casing Recess on Heat Transfer and Stage Efficiency in Axial Turbines," *ASME* J. Turbomachinery, **121**, pp. 683-693, Paper No. 98-GT-369.
9. Prasad, A., and Wagner, J. H., 2000, "Unsteady Effects in Turbine Tip Clearance Flows," *ASME* Paper No. 2000-GT-0444.
10. Rao, N. M., and Camci, C., 2004, "A Flow Visualization Study of Axial Turbine Tip Desensitization by Coolant Injection from a Tip Trench," *ASME* Paper No. IMECE2004-60943.
11. Lakshminarayana, B., Camci, C., Halliwell, I., and Zaccaria, M., 1996, "Design and Development of a Turbine Research Facility to Study Rotor-Stator Interaction Effects," International Journal of Turbo and Jet Engines, **13**, pp.155-172.
12. Camci, C., 2004, Experimental and Computational Methodology for Turbine Tip De-sensitization. *VKI Lecture Series 2004-02*, "Turbine Blade Tip Design and Tip Clearance Treatment," 2004.
13. Sharma, O. P., and Butler, T. L., 1987, "Predictions of Endwall Losses and Secondary Flows in Axial Turbine Cascades," *ASME* J. of Turbomachinery, **109**, pp. 229-236.
14. Langston, L. S., 1990, "Crossflows in a Turbine Cascade Passage," *Journal of Engineering for Power*, **102**, pp. 866-874.
15. Gregory-Smith, D. G., Graves, C. P., Walsh, J. A., 1988, "Growth of Secondary Losses and Vorticity in an Axial Cascade," *ASME* J. of Turbomachinery, **110**, pp. 1-8.
16. Xiao, X., McCarter, A. A., and Lakshminarayana, B., 2001, "Tip Clearance Effects in a Turbine Rotor: Part 1-Pressure Field and Loss," *ASME* J. of Turbomachinery, **123**, pp. 296-304.
17. Rao, N. M., and Camci, C., 2004, "Axial Turbine Tip Desensitization by Injection from a Tip Platform Trench. Part 1- Effect of Injection Mass Flow Rate," *ASME* Paper No. GT2004-53256.

18. Rao, N. M., and Camci, C., 2004, “Axial Turbine Tip Desensitization by Injection from a Tip Platform Trench. Part 2- Leakage Flow Sensitivity to Injection Location,” *ASME* Paper No. GT2004-53258.